NJC

Accepted Manuscript

Volume 40 | Number 1 | January 2016 | Pages 1–846

NJC

New Journal of Chemistry
www.rsc.org/njc

A journal for new directions in chemistry

ISSN 1144-0546

ROYAL SOCIETY OF CHEMISTRY

PAPER
Jason B. Benedict et al
The role of atropisomers on the photo-reactivity and fatigue of
diarylethene-based metal–organic frameworks

cnrs

ROYAL SOCIETY OF CHEMISTRY

rsc.li/njc

Effects of pore structure of MgO-templated mesoporous carbon on its supported Pt catalysts for reductive alkylation of p-aminodiphenylamine with methyl isobutyl ketone

YU Wenlong, YU Shitao[#], DING Junwei[*], CHENG Qiuzhen, LIU Fusheng

College of Chemical Engineering, Qingdao University of Science and Technology, 53 Zhengzhou Road,

Qingdao 266042, Shandong, China

Abstract: Mesoporous carbon (MC) was prepared by nano-MgO template method and used as support for the preparation of a Pt-based reductive alkylation catalyst. N_2 physical adsorption-desorption, scanning electron microscopy, transmission electron microscopy and X-ray diffraction were used to characterize the carbon supports and supported Pt catalysts. The effects of pore structure of the Pt/MC catalyst on its performance for reductive alkylation of p-aminodiphenylamine with methyl isobutyl ketone were investigated. The results show that the surface area and pore structure of the MgO-templated mesoporous carbons can be modulated directionally by varying the size of nano-MgO particles and the MgO/PF mass ratio. The catalytic activity and stability of the catalysts for N-(1,3-dimethylbutyl)-N'-phenyl-p-phenylenediamine synthesis increases with increased pore size of the mesoporous carbons. Complete conversion of p-ADPA and 100% selectivity to 6PPD were obtained over Pt/MC50(1/1) within 4 hours, which could maintain high catalytic activity after reused 10 times. The characterization results indicate that there was obviously decreasing of the BET specific surface area, pore volume and Pt specific surface area of all used catalysts comparing with the fresh catalysts, and the trend was more obvious with the decrease of catalyst pores, which should be the primary reason for the degradation of catalytic performance.

Key words: Mesoporous carbon, Nano-MgO template, Pt-based catalyst, Pore structure, Reductive alkylation

1. Introduction

Reductive alkylation of amine compounds is commercially practiced in a variety of industrial processes for the manufacture of higher alkylated (secondary and tertiary) amine derivatives, which find applications as intermediates in fine chemicals and specialty products[1-4]. An important example of this class of reaction is the reductive alkylation of p-aminodiphenylamine (p-ADPA) to N-(1,3-dimethylbutyl)-N'-phenyl-p-phenylenediamine (6PPD), which is widely used for rubber antioxidant[5-8]. This reaction goes through a condensation dehydration reaction between p-ADPA and methyl isobutyl ketone (MIBK) to form the imine (Schiff base), followed by hydrogenation to 6PPD in the presence

of metal catalysts[9-11].

Ordinary copper catalysts were employed in industrial processes to manufacture the 6PPD due to their cheap costs, however, these catalysts have the obvious defects, such as low-activity and selectivity resulting in harsh reaction conditions and ketone converting into alcohol, copper-leaching aggravating rubber aging. Supported noble metal catalysts[12, 13] were then developed to overcome the disadvantages of traditional copper-based catalysts, synthesizing 6PPD with high quality and efficiency. Most of the previous works on reductive alkylation were focused on the development of hydrogenated active site with the aim of improving the catalytic activity and selectivity[14-17]. However, the research on the influence of support structural characteristics is rarely reported to the best of our knowledge.

Support is one of the most important parts of heterogeneous catalyst[18-20], which plays a vital role in loading active components and improving their dispersion and also provides a space for the reactants to react. Catalyst support affects the diffusion and adsorption of the reactants directly determining the accessibility of the reactants with the active sites[21-25] and thereby, it has a significant effect on the reductive alkylation catalytic activity. The conventional used reductive alkylation catalyst support is activated carbon but it has relatively small pore size and narrow pore channels, which is not conductive to the active component dispersion and macromolecular reaction.

Mesoporous carbons have attracted a lot of attention in the fields of sorption and separation of macromolecules, catalysis, and synthesis of nanomaterials because of their high surface area and tunable pore diameters at the nanoscale[26-29]. A hard-template method[30-33] is generally used in the preparation of mesoporous carbon materials. The pore structure of the carbon materials can be easily adjusted by varying the template types and sizes. As a typical kind of hard-template mesoporous carbons, MgO-templated mesoporous carbon[34-37] has become commercially available due to the MgO-template recoverability and easy removability by washing with a diluted acidic solution.

In this work, mesoporous carbons (MC) with different pore diameters and surface areas were prepared by using nano-MgO as a hard template and phenolic resin (PF) as a carbon precursor. The effects of pore structure on the performance of supported Pt-based catalyst, Pt/MC, for reductive alkylation to 6PPD were investigated.

2. Experimental

2.1. Preparation of mesoporous carbon

Phenolic resin was purchased from Jinan Shengquan Group Share Holding Co., Ltd. (Jinan, China), and nano-MgO was provided by Nanjing Hongde nanomaterials Co., Ltd. (Nanjing, China). Three nano-MgO samples with particle size of 15 nm, 30 nm and 50 nm were used. The MgO/PF ratio was defined as the

mass ratio of nano-MgO to phenolic resin.

A typical process for preparation of the MgO-templated mesoporous carbon material with a MgO/PF ratio of 1/1 is described as follows. Phenolic resin (10 g) was dissolved in 50 ml of ethanol (AR, Sinopharm Chemical Reagent Co., Ltd., Shanghai, China). Nano-MgO (10 g) was dispersed in 100 ml of ethanol via ultrasonic treatment. The ethanol-phenolic resin solution was then added dropwise to the ethanol-MgO dispersion liquid. The mixture was stirred for 12 h at room temperature and then dried in a vacuum oven at 50 °C for 12 h. The obtained solid was carbonized in a pipe furnace (Hefei Kejing materials technology Co., Ltd., Hefei, China) at 900 °C for 2 h, in a flow of high purity N_2 gas (99.999%, Qingdao Heli Gases Co., Ltd., Qingdao, China) at a rate of 20 ml/min. The heating rate up to 900 °C was 3 °C /min. From carbon-coated MgO particles thus obtained, template MgO was dissolved out using 10 w% H_2SO_4 (AR, Sinopharm Chemical Reagent Co., Ltd., Shanghai, China) aqueous solution (40 ml H_2SO_4 aqueous solution / g MgO) at 50 °C for 5 h. The dissolution process of MgO was repeated 3 times until the magnesium ion in the filtrate could not be detected by ICP-OES. The solid was then filtered and washed with deionized water until the pH reached to 7. The mesoporous carbons, which were obtained by drying at 110 °C for 24 h, were designated as MC15, MC30, MC50 and MC50, where MC refers to mesoporous carbon, 15, 30 and 50 refer to the size (nm) of the MgO used, 1/3, 1/1, and 3/1 refer to the MgO/PF mass ratio.

2.2. Preparation of catalyst

Mesoporous carbon supported Pt catalysts with a nominal Pt loading of 3.0 w% were prepared by the conventional impregnation method. Prior to impregnation, the synthesized MgO-templated mesoporous carbon was pretreated with 10 % HNO_3(AR, Sinopharm Chemical Reagent Co., Ltd., Shanghai, China) at 50 °C for 5h, followed by washing with distilled water until the pH reached to 7 and then dried under vacuum at 110 °C for 12 h. The point of zero charge (PZC) of all HNO_3 treated supports determined by mass titration was controlled at about 5 [38]. 15 ml of H_2PtCl_6 (Sino-Platinum Metals Corp. Ltd.) aqueous solution (0.01 g/ml) was then added dropwise into 50 ml of aqueous suspension containing 5 g of pretreated mesoporous carbon, and then the pH of the suspension was adjusted to 10 by adding NaOH (AR, Sinopharm Chemical Reagent Co., Ltd., Shanghai, China) aqueous solution. The precipitated $Pt(OH)_4$ was reduced by $NaBH_4$(AR, Sinopharm Chemical Reagent Co., Ltd., Shanghai, China) at room temperature, which was then washed with deionized water until the pH of the filtrate was 7 and no chloride ions could be observed in the filtrate by the $AgNO_3$ titration method. This sample was then dried under the vacuum at 110 °C for 12 h. The catalyst was designated as Pt/MC, where MC can be represented by MC15, MC30 or MC50.

As a comparison, Pt/AC catalyst with a nominal Pt loading of 3.0 w% were prepared using the same method as mentioned above. A commercial activated carbon (Calgon Carbon Corp. Ltd.) was used as the

catalyst support.

2.3. Catalyst characterization

Scanning electron microscopy (SEM) was performed on a JSM-7500Fmicroscope (JEOL Ltd.) with an accelerating voltage of 8.0 kV. The samples were then gold coated by cathodic sputtering. Transmission electron microscopy (TEM) images of the catalysts were obtained using a JEM-2100F microscope(JEOL Ltd.) operating at an accelerating voltage of 200 kV. The samples for TEM were prepared by dropping the ethanol suspensions of the catalysts on copper grids. The powder X-ray diffraction (XRD) patterns of the samples were recorded on D/max2500 diffractometer (Rigaku Corp.) with Cu K_α radiation at 40 kV and 150 mA. The metal content of the catalysts were quantitatively determined by inductively coupled plasma atomic emission spectroscopy (ICP-OES) using a Varian715-ES (Varian Inc.). The surface area and pore structure of the catalysts were determined by N_2 physical adsorption-desorption using a ASAP 2020 surface area analyzer (Micromeritics Instrument Corp.).The surface area of the samples was calculated by the BET equation. The specific surface area of Pt supported on the carbon was determined by CO chemical adsorption using an AutoChemII 2920 analyzer (Micromeritics Instrument Corp.).

2.4. Catalyst performance

The reductive alkylation to 6PPD was carried out in an autoclave (Weihai Huixin Chemical Mechanic Corp. Ltd.) which was made of 316L stainless steel with a working volume of 500 ml. The reaction conditions were as follows: p-ADPA = 50 g, MIBK = 109 g, catalyst = 0.5 g, T = 373 K, P = 2.5 MPa (pure H_2, 99.9%, Qingdao Heli Gases Co., Ltd., Qingdao, China), stirring speed = 700 r/min. The catalyst was recycled by filtration after reaction. The reaction products were analyzed by gas chromatography (Agilent7820A) equipped with an FID detector and a capillary column HP-5(30 m×0.32 mm×0.25 μm).

The conversion of p-ADPA and selectivity of 6PPD can be calculated by the following equations respectively：

$$X = \frac{C_{\text{p}-\text{ADPA}}^0 - C_{\text{p}-\text{ADPA}}}{C_{\text{p}-\text{ADPA}}^0} \times 100\%$$

$$S = \frac{C_{6\text{PPD}}}{C_{\text{p}-\text{ADPA}}^0 - C_{\text{p}-\text{ADPA}}} \times 100\%$$

where X is the p-ADPA conversion, S is the 6PPD selectivity, C^0 and C denote the initial and final mole fraction, respectively.

3.   Results and discussion

### 3.1. Structural properties of mesoporous carbon and catalyst

The effects of nano-MgO particle size and MgO/PF ratio on the pore structure and surface area of the prepared mesoporous carbons were studied. Table 1 gives the physical properties of prepared mesoporous carbons and commercial activated carbon. Sample C-none, which was directly carbonized with PF without a nano-MgO template, mainly consisted of micropores, with a minimal specific surface area of 22 m^2/g. At the same MgO/PF ratio, the total specific surface area and pore volume of the mesoporous carbons decreased with an increased particle size of the nano-MgO templates. However, using the same nano-MgO template, the total specific surface area and pore volume of prepared mesoporous carbons increased with an increased MgO/PF ratio. From the pore size distribution (Fig.1) and the data in Table 1, a sharp pore size distribution at about 6 nm for the MC15 was displayed. As the nano size of MgO templates increased, the pore size of MC30 and MC50 became larger than that of MC15, having pore size distribution with maxima at 10 and 17 nm, respectively. Furthermore, for all the mesoporous carbons prepared at different MgO/PF ratios with 30 nm nano-MgO as templates, the pore diameters were approximately 10nm, which indicates that the amount of nano-MgO does not affect the pore size of the mesoporous carbon significantly. All these results demonstrate that the surface area and pore structure of the MgO-templated mesoporous carbon samples can be modulated by varying the size of nano-MgO particles and the MgO/PF ratio.

Table 1 Textural properties of different carbon samples.

| Samples	MgO size / nm	MgO/PF mass ratio	S_{BET} / m^2g^{-1}	S_{Micro} [a]/ m^2g^{-1}	V_{Total} / cm^3g^{-1}	V_{Micro} [a]/ cm^3g^{-1}	D_{de} [b]/ nm
C-none	--	--	22	20	0.01	0.01	--
MC15(1/1)	15	1/1	661	58	0.65	0.03	5.9
MC30(1/3)	30	1/3	532	152	0.61	0.07	9.8
MC30(1/1)	30	1/1	610	136	0.63	0.06	10
MC30(3/1)	30	3/1	832	145	1.06	0.08	9.7
MC50(1/1)	50	1/1	348	135	0.59	0.08	17
AC	--	--	1570	551	0.92	0.23	2.3

a Calculated by t-plot method.

b The peak pore size in the pore distribution calculated by BJH desorption method.
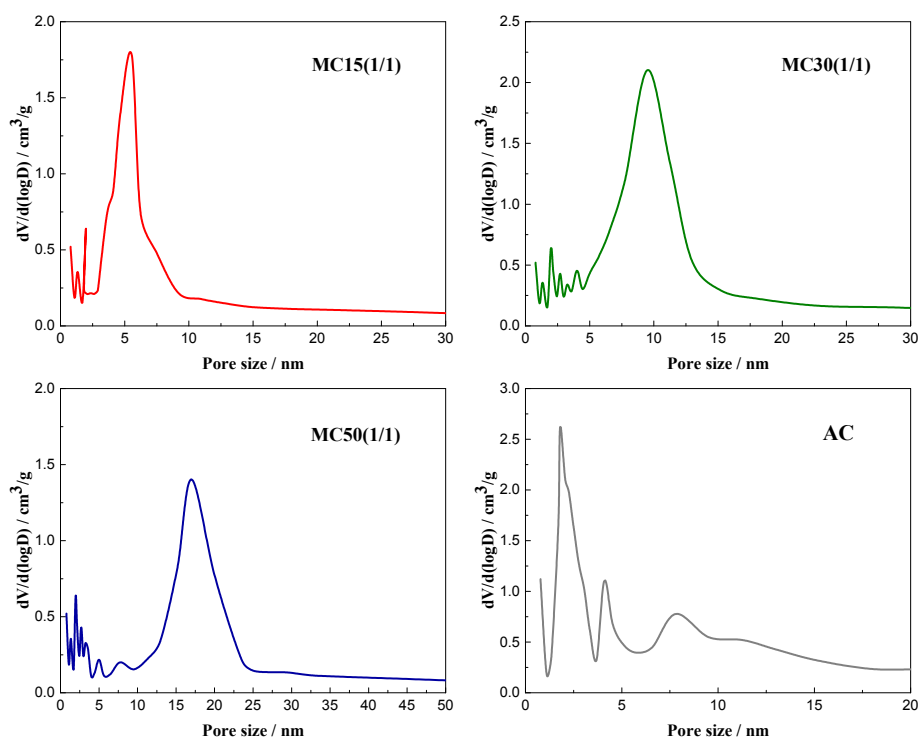
Fig. 1 Pore size distribution of various mesoporous carbons and activated carbon.

In order to explore the surface structure and morphology of various carbon samples, SEM characterization was carried out. Fig.2 shows the SEM images of different carbon material samples. It was observed that the carbon marked as C-none (Fig. 2a) which was directly carbonized with PF without a nano-MgO template had a flat surface and a non-porous structure. The porous carbons prepared exhibit alveolate structures as shown in Fig. 2b to 2e when nano-MgO templates were used. The amount of pores increased noticeably with the addition of MgO as shown in Fig. 2b to 2f. At the same MgO/PF ratio, larger pores could form on the carbon material using bigger sized MgO-template (Fig. 2b, Fig. 2d and Fig. 2f), replicating the size of MgO nanocrystals correspondingly. Under high magnification conditions(Fig. 2h and Fig. 2i), it can be seen that these larger pore structures are connected with each other though smaller pores on all of the MgO-templated mesoporous carbons constructing interconnected carbon walls, which can provide ideal channels for the diffusion of reactant molecules. In contrast, the commercial activated carbon shows less mesoporous-macroporous morphology from Fig. 2g.
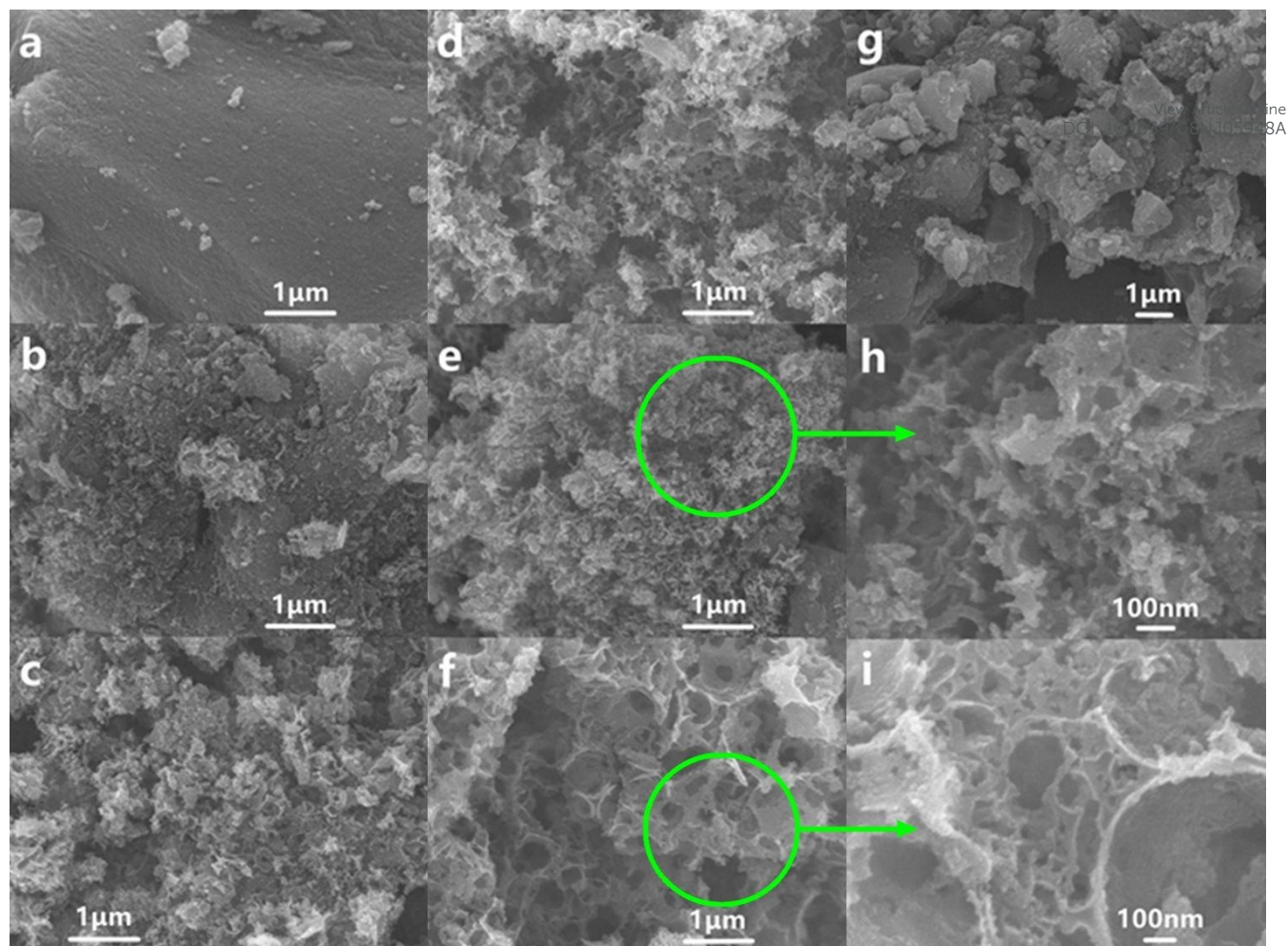
Fig. 2 SEM images of carbon samples (a:C-none; b: MC15(1/1); c: MC30(1/3); d: MC30(1/1); e: MC30(3/1); f: MC50(1/1); g: commercial activated carbon; h and i: the interior of MC30(3/1) and MC50(1/1) with high magnification).

Fig.3 presents the XRD patterns of MC30 (1/1) and activated carbon. It was observed that both carbon material samples had only broad diffraction peaks at $2\theta = 25°$ attributed to the amorphous carbon and no other characteristic diffraction peaks were found, which indicates that the MgO-templated mesoporous carbon prepared at 900 ℃ had negligible graphitization.
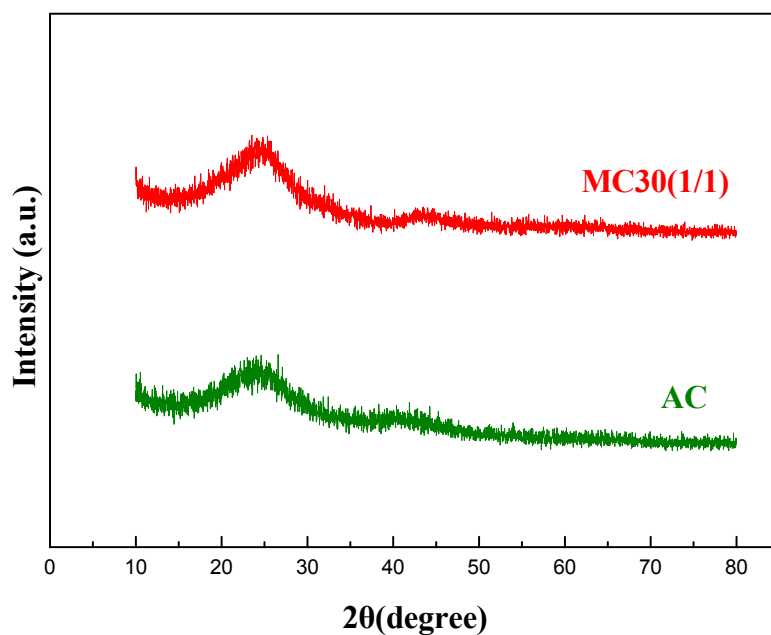
Fig. 3 XRD patterns of MC30(1/1) and the commercial activated carbon(AC).
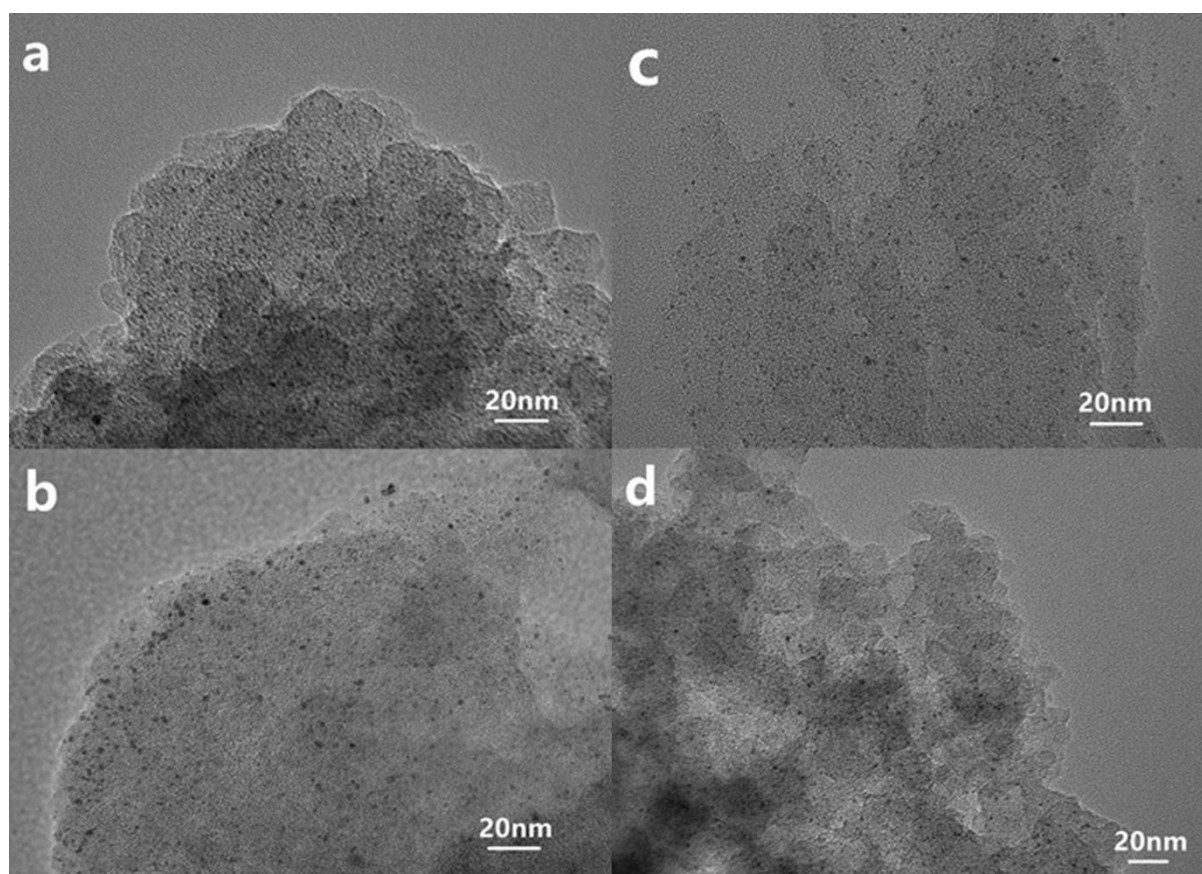
Fig. 4 TEM images of fresh Pt/MC15 (1/1) (a), MC30 (1/1) (b), Pt/MC50 (1/1) (c) and Pt/AC (d).

The TEM images of the Pt catalysts with different carbon supports are given in Fig.4. It was noted that the highly dispersed Pt nanoparticles,1-3 nm in size, were uniformly distributed within the supports and no obvious nanoparticles aggregation was observed in all the catalyst samples. The XRD result is in accordance with the conclusion of TEM analysis. It was obvious from the XRD patterns (Fig. 5) that all the catalysts

had only broad diffraction peaks at $2\theta = 25°$ attributed to the amorphous carbon and no characteristic

diffraction peaks of Pt were found, which was possibly due to Pt nanoparticles being highly dispersed into

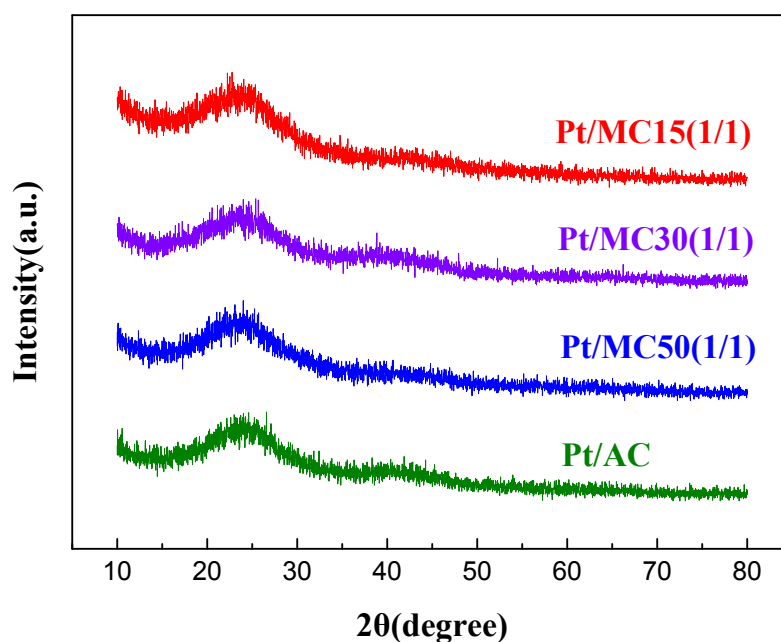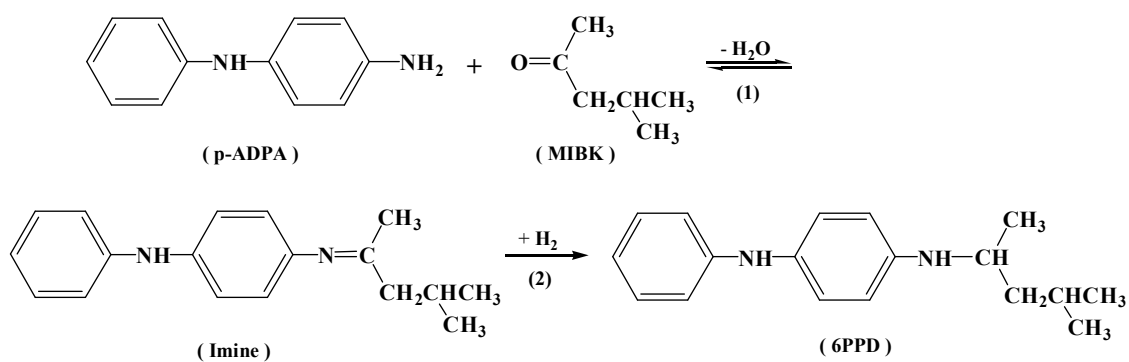amorphous state both within mesoporous carbons and commercial activated carbon.

Fig. 5 XRD patterns of fresh Pt/MC15(1/1) , MC30(1/1) , Pt/MC50(1/1) and Pt/AC.

3.2. Performance of Pt/MC catalyst for reductive alkylation

Scheme 1. Reaction pathways for the synthesis of N-(1,3-dimethylbutyl)-N'-phenyl-p-phenylenediamine (6PPD) .

The reaction for the synthesis of N-(1,3-dimethylbutyl)-N'-phenyl-p-phenylenediamine (6PPD) is

shown in Scheme. 1. The activities of all catalysts are shown in Table 2. 99.5% conversion of p-ADPA was

obtained over Pt/MC15(1/1) with a selectivity (99.2%) to 6PPD, while p-ADPA were completely converted

both over Pt/MC30 and Pt/MC50 with higher selectivity close to 100%. It is obvious that the reaction time

decreased with increased pore size of catalyst supports from 6 h to 4 h. However, it should be noted that the

surface areas of MC30s differing from each other because of the differences in the MgO/PF ratios, had little

effect on catalytic performance. More specifically, the correlation between the reaction rate and pore size of

catalyst supports is given in Fig. 6. It is obvious that the p-ADPA conversion rate increased linearly with the pore size of mesoporous carbon increases. For comparison，a lower conversion of p-ADPA (98.5%) and a lower selectivity (98.2%) to 6PPD with the reaction time extended to 8 h were obtained over commercial activated carbon supported Pt catalyst. The main by-products were N-(1,3-dimethylbutyl)-N'-cyclohexane-p-phenylenediamine and aniline, which were derived from the hydrogenation of 6PPD and the hydrogenolysis of imine, respectively.

Table 2 Catalytic performance of Pt catalysts supported on various mesoporous carbon and activated carbon in the synthesis of 6PPD[a].

Catalyst	Reaction time / h	p-ADPA conversion / %	Selectivity / %		
			6PPD	Imine	Others
Pt/MC15(1/1)	6	99.5	99.2	0.5	0.3
Pt/MC30(3/1)	4.5	100	99.8	0.1	0.1
Pt/MC30(1/1)	4.5	100	99.9	0	0.1
Pt/MC30(1/3)	4.5	100	99.8	0.2	0
Pt/MC50(1/1)	4	100	100	0	0
Pt/AC	7.5	98.5	98.2	0.8	1.0

[a] Reaction condition: p-ADPA = 50 g, MIBK = 109 g, catalyst = 0.5 g, T = 373 K, P = 2.5 MPa (pure H_2), stirring speed = 700 r/min.
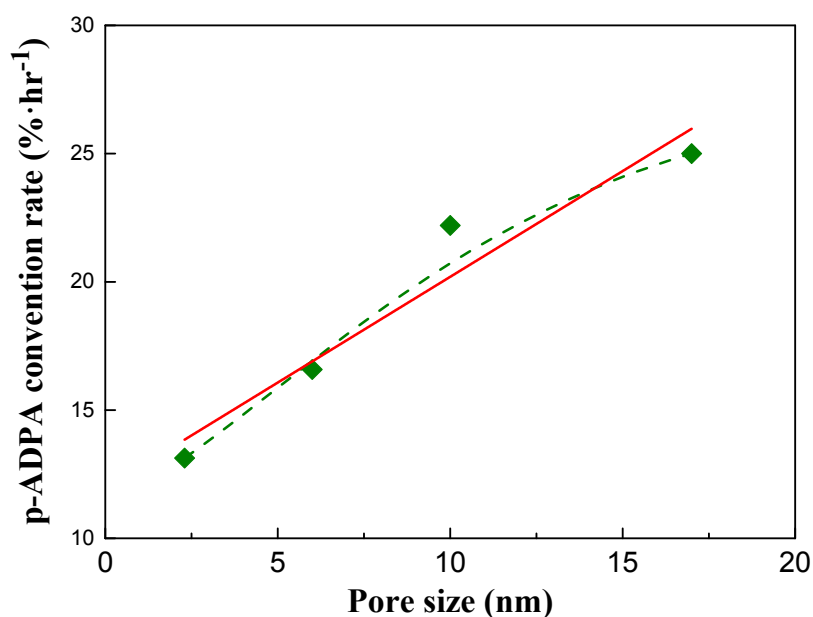

Fig. 6 Relationship between catalytic activity and pore size of catalyst supports. P-ADPA conversion rate was calculated by the following equation：$W = \frac{X_{p\text{-}ADPA}}{t}$, where W is the p-ADPA conversion rate, X is the p-ADPA conversion, t is the reaction time.

The stability of catalysts in reductive alkylation reactions of p-ADPA with MIBK was investigated via the reuse of catalysts under the same reaction conditions as mentioned above. As shown in Fig. 7, the p-ADPA conversion remained above 96% after the Pt/MC50 (1/1) reused 10 times. However, varying degrees of decrease of p-ADPA was obtained over the rest of catalysts with the increase of catalysts reused times. In particular, the p-ADPA conversion reduced to 73.5 % after the Pt/AC reused 10 times. All of the above results show that the pore structure of the carbon support significantly affects the performance of the supported Pt catalyst.
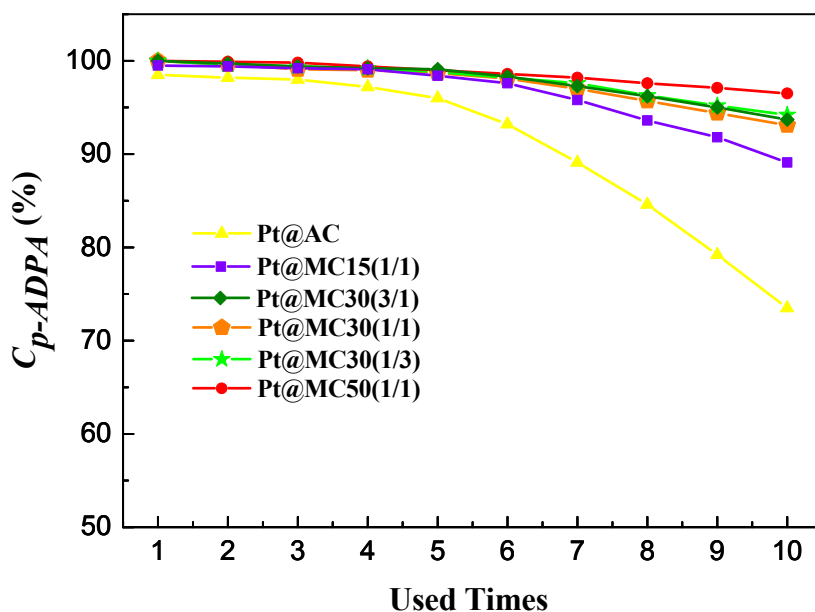
Fig. 7 Recyclability of Pt catalysts supported on various mesoporous carbon and activated carbon in the synthesis of 6PPD. Reaction condition: p-ADPA = 50 g, MIBK = 109 g, catalyst = 0.5 g, T = 373 K, P = 2.5 MPa (pure H_2), stirring speed = 700 r/min.

3.3. Catalyst deactivation
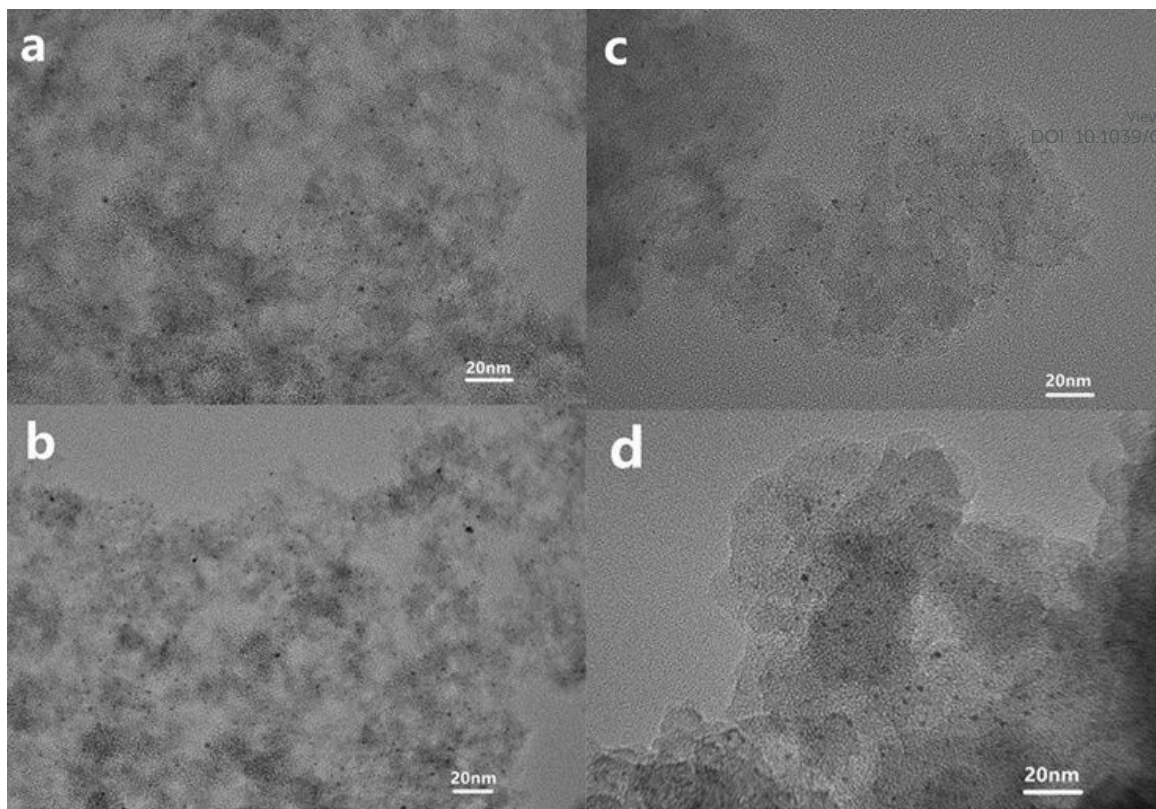
Fig. 8 TEM images of used Pt/MC15(1/1) (a), MC30(1/1) (b), Pt/MC50(1/1) (c) and Pt/AC (d).

Fig. 8. shows the TEM images of catalysts reused 10 times, respectively. It is seen that the highly dispersed Pt nanoparticles were still distributed on the carbon supports and no nanoparticles sintering was observed, just like fresh catalysts.

Table 3 Pt content of fresh and used catalysts.

Catalyst samples	Pt content / %
Fresh Pt/MC15(1/1)	2.92
Fresh Pt/MC30(1/1)	2.93
Fresh Pt/MC50(1/1)	2.92
Fresh Pt/AC	2.94
Used Pt/MC15(1/1)	2.88
Used Pt/MC30(1/1)	2.88
Used Pt/MC50(1/1)	2.89
Used Pt/AC	2.90

Pt content of fresh and used catalysts are listed in Table 3. It can be seen that very slight Pt loss was observed for all the used catalysts, which won't significantly reduce the catalytic performance.

Table 4 Textural properties of the fresh and used catalysts.

Catalyst samples	S_{BET} / m^{2}g^{-1}	V_{total} / cm^{3}g^{-1}	S_{Pt} / m^{2}g^{-1}

Fresh Pt/MC15(1/1)	643	0.64	79.33
Fresh Pt/MC30(1/1)	585	0.62	81.03
Fresh Pt/MC50(1/1)	331	0.57	80.55
Fresh Pt/AC	1502	0.90	84.67
Used Pt/MC15(1/1)	514	0.51	61.88
Used Pt/MC30(1/1)	495	0.52	67.05
Used Pt/MC50(1/1)	314	0.53	74.82
Used Pt/AC	766	0.46	38.01

Furthermore, N_2 physical adsorption and CO chemical adsorption characterization of fresh and used catalysts were carried out. The BET specific surface area and pore volume of used catalysts all decreased obviously comparing with fresh catalysts, and the trend was more obvious with the decrease of catalyst pores. Correspondingly, Pt specific surface area of used catalysts had a similar trend. According to the results of catalyst characterization, it can be concluded that during the reductive alkylation of p-ADPA with MIBK, narrow pore structure would hinder mass transfer and diffusion of reactants and products, accentuating the deposition and blockage of organic matter in the pores, covering active centers, which should be the primary reason of lower catalytic performance.

4.   Conclusions

The preparation of the nano-MgO templated mesoporous carbon with different pore structures as well as the effects of pore structure on the performance of supported Pt catalysts for reductive alkylation of p-aminodiphenylamine with methyl isobutyl ketone were investigated. The pore structure and surface area of the mesoporous carbon can be controlled by modulating the size of nano-MgO and the mass ratio of MgO/PF. However, the surface areas of mesoporous carbons differing from each other because of the differences in the MgO/PF mass ratio had little effect on catalytic performance. The catalytic activity and stability of catalysts for N-(1,3-dimethylbutyl)-N'-phenyl-p-phenylenediamine synthesis increases with increased pore size of the mesoporous carbons. Complete conversion of p-ADPA and 100% selectivity to 6PPD were obtained over Pt/MC50(1/1) within 4 hours, which could maintain high catalytic activity after reused 10 times. The BET specific surface area and Pt specific surface area of used catalysts all decreased obviously comparing with fresh catalysts, and the trend was more obvious with the decrease of catalyst pores. Narrow pore structure would hinder mass transfer and diffusion of reactants and products, accentuating the deposition and blockage of organic matter in the pores, covering active centers, which should be the primary reason for the degradation of catalytic performance.

Acknowledgements

References

1. F. Cataldo, *European Polymer Journal*, 2002, **38**, 885-893.
2. F. Cataldo, *Polymer Degradation and Stability*, 2018, **147**, 132-141.
3. Z. Cibulková, P. Šimon, P. Lehocký and J. Balko, *Polymer Degradation and Stability*, 2005, **87**, 479-486.
4. I. Puškárová, M. Šoral and M. Breza, *Chemical Physics Letters*, 2015, **639**, 78-82.
5. P. Rapta, A. Vargová, J. Polovková, A. Gatial, L. Omelka, P. Majzlík and M. Breza, *Polymer Degradation and Stability*, 2009, **94**, 1457-1466.
6. I. Puškárová and M. Breza, *Polymer Degradation and Stability*, 2016, **128**, 15-21.
7. A. V. Babkin, A. F. Asachenko, D. V. Uborsky, D. S. Kononovich, V. V. Izmer, V. A. Kudakina, V. A. Shnaider, N. E. Shevchenko and A. Z. Voskoboynikov, *Mendeleev Communications*, 2016, **26**, 555-557.
8. A. Gatial, J. Polovková, I. Kortišová and M. Breza, *Vibrational Spectroscopy*, 2007, **44**, 1-8.
9. H.L.Merten and L.M.Baclawski ,US4900868, **1990**.
10. R. M. D.Sidocky and D. K. Parker, US4463191,**1984**.
11. M. A. Fox and J. K. Whitesell,*Organic Chemistry*, Jones and Bartlett Publishers, Boston, MA, 1994.
12. F.N.Schwettmann ,US3384664, **1968**.
13. K.Tada,N.Kodear and M.Hanai, JP82123148, **1982**.
14. Q. Zhang, F. Feng, C. Su, W. Xu, L. Ma, C. Lu and X. Li, *RSC Advances*, 2015, **5**, 66278-66285.
15. W. Xu, J. Ni, Q. Zhang, F. Feng, Y. Xiang and X. Li, *Journal of Materials Chemistry A*, 2013, **1**, 12811-12817.
16. Q. F. Zhang, J. C. Wu, C. Su, F. Feng, Q. L. Ding, Z. L. Yuan, H. Wang, L. Ma, C. S. Lu and X. N. Li, *Chinese Chemical Letters*, 2012, **23**, 1111-1114.
17. N. G. Patil, D. Roy, A. S. Chaudhari and R. V. Chaudhari, *Industrial & Engineering Chemistry Research*, 2007, **46**, 3243-3254.
18. K. Chandra Mouli, K. Soni, A. Dalai and J. Adjaye, *Applied Catalysis A: General*, 2011, **404**, 21-29.
19. G. Zhao, T. S. Zhao, J. Xu, Z. Lin and X. Yan, *International Journal of Hydrogen Energy*, 2017, **42**, 3325-3334.
20. K. Cheng, M. Virginie, V. V. Ordomsky, C. Cordier, P. A. Chernavskii, M. I. Ivantsov, S. Paul, Y. Wang and A. Y. Khodakov, *Journal of Catalysis*, 2015, **328**, 139-150.
21. D. Song and J. Li, *Journal of Molecular Catalysis A: Chemical*, 2006, **247**, 206-212.
22. Y. Zhou, G. Lan, B. Zhou, W. Jiang, W. Han, H. Liu and Y. Li, *Chinese Journal of Catalysis*, 2013, **34**, 1395-1401.
23. Y. Zhao, Z. Guo, H. Zhang, B. Peng, Y. Xu, Y. Wang, J. Zhang, Y. Xu, S. Wang and X. Ma, *Journal of Catalysis*, 2018, **357**, 223-237.
24. M. Nurunnabi and S. Q. Turn, *Fuel Processing Technology*, 2015, **130**, 155-164.

25. P. G. Blakeman, E. M. Burkholder, H.-Y. Chen, J. E. Collier, J. M. Fedeyko, H. Jobson and R. R. Rajaram, *Catalysis Today*, 2014, **231**, 56-63.
26. M. Enterría and J. L. Figueiredo, *Carbon*, 2016, **108**, 79-102.
27. J. Wei, Y. Deng, J. Zhang, Z. Sun, B. Tu and D. Zhao, *Solid State Sciences*, 2011, **13**, 784-792.
28. W. Li, Q. Yue, Y. Deng and D. Zhao, *Advanced Materials*, 2013, **25**, 5129-5152.
29. T.-Y. Ma, L. Liu and Z.-Y. Yuan, *Chemical Society Reviews*, 2013, **42**, 3977-4003.
30. M. Inagaki, M. Toyoda, Y. Soneda, S. Tsujimura and T. Morishita, *Carbon*, 2016, **107**, 448-473.
31. R. Ryoo, S. H. Joo, M. Kruk and M. Jaroniec, *Advanced Materials*, 2001, **13**, 677-681.
32. J. Lee, S. Han and T. Hyeon, *Journal of Materials Chemistry*, 2004, **14**, 478-486.
33. R. Ryoo, S. H. Joo and S. Jun, *The Journal of Physical Chemistry B*, 1999, **103**, 7743-7746.
34. T. Morishita, T. Tsumura, M. Toyoda, J. Przepiórski, A. W. Morawski, H. Konno and M. Inagaki, *Carbon*, 2010, **48**, 2690-2707.
35. H. Orikasa and T. Morishita, *Carbon*, 2013, **52**, 621.
36. T. Morishita, L. Wang, T. Tsumura, M. Toyoda, H. Konno and M. Inagaki, *Carbon*, 2010, **48**, 3001.
37. B. Acevedo and C. Barriocanal, *Microporous and Mesoporous Materials*, 2015, **209**, 30-37.
38. J. S. Noh and J. A. Schwarz, *Carbon*, 1990, **28**, 675-682.

Graphical Abstract